NBSIR 75-659

A New Mode of Chipping Fracture in Brittle Solids, and Its Application in a Model for Wear Under Fixed Abrasive Conditions
I. Mode of Chipping Fracture
II. Wear Model

B. R. Lawn

Inorganic Materials Division
Institute for Materials Research
National Bureau of Standards
Washington, D. C. 20234

February 1975

Interim Report for Period July 1, 1974 through June 30, 1975

Prepared for
Department of the Navy
Office of Naval Research
Arlington, Virginia 22217

Lawn, B. R., Swain, M. V., Phillips, K.,

On the mode of chipping fracture in brittle solids, J. Mater Sci. Lett. 10, 1236-1239 (1975).

313.

16336

NBSIR 75-659

Lawn, B. R., A model for the wear of brittle solids under fixed abrasive conditions, Wear Short Commun. 33, 369-372 (1975).

NBSIR 75-659

340

16335

NBSIR 75-659

A NEW MODE OF CHIPPING FRACTURE IN BRITTLE SOLIDS, AND ITS APPLICATION IN A MODEL FOR WEAR UNDER FIXED ABRASIVE CONDITIONS

I. MODE OF CHIPPING FRACTURE

II. WEAR MODEL

B. R. Lawn

Inorganic Materials Division
Institute for Materials Research
National Bureau of Standards
Washington, D. C. 20234

February 1975

Interim Report for Period July 1, 1974 through June 30, 1975

Prepared for
Department of the Navy
Office of Naval Research
Arlington, Virginia 22217

U. S. DEPARTMENT OF COMMERCE, Frederick B. Dent, Secretary
NATIONAL BUREAU OF STANDARDS, Richard W. Roberts, Director

I. On the Mode of Chipping Fracture in Brittle Solids

Chipping processes in brittle solids, despite their unquestionable relevance to a diversity of technologies from ceramics finishing to geological engineering, are not well understood at the fundamental level. Some recent studies of microfracture patterns beneath standard hardness indenters do, however, provide some insight into the problem[1,2], and it is our objective here to indicate how this insight may be applied to construct a physical model of chipping fracture. Essentially, the picture which emerges is that depicted in Fig. 1: (i) Upon loading the indenter, a confined zone of irreversible (plastic) deformation forms about any sharp points or corners (thereby accounting for the residual hardness impression), from which "median vent" cracks first initiate and subsequently propagate radially outward along suitable planes of symmetry (e.g. as defined by the diagonals of a pyramid indenter, or by preferred cleavage planes) containing the contact axis; (ii) Upon unloading the indenter, the median vents close up, but, just prior to complete removal, "lateral vent" cracks initiate and extend laterally from the deformation zone toward the specimen surface. Of the two types of cracking it is clearly the second which relates more directly to brittle chipping.

Yet up till now a detailed fracture mechanics analysis has been attempted only for the median vent system. This system is relatively well defined, since the indentation stress field, which uniquely determines the extent of crack growth[1], can reasonably be represented in terms of the classical Boussinesq field for normal point loading[2,3]. On the basis of the fundamental Griffith energy-balance condition for fracture[4], it may readily be argued that brittle cracks will generally tend to follow trajectories of the lesser principal stresses within the indentation field, such that the path maintains near-orthogonality to a component of major tension: the best studied illustration of this principle is the Hertzian cone crack [5, 6], which, in the absence of any deformation-induced nucleation center, initiates from an incipient surface flaw and flares downward into the specimen. In the scheme of Fig. 2, in which the principal stresses are defined such that $\sigma_{11} \geqslant \sigma_{22} \geqslant \sigma_{33}$ (positive values denoting tension) nearly everywhere, median vent geometry may be specified in terms of families of σ_{11} and σ_{33} trajectories, cone crack geometry in terms of families of σ_{22} and σ_{33} trajectories.

The conditions under which the lateral vents form are, unfortunately, less easily modelled. Since the lateral system operates only as the indenter is withdrawn from the specimen surface it is evident that the driving force for propagation must originate from some <u>residual stress field</u> associated with the irreversible deformation zone. This conclusion is substantiated by microscopic investigation of the damage patterns as a function of indenter geometry (e.g. "sharp" or "blunt"): in general, the extent of lateral venting is found to increase markedly with expanding zone size. A graphic illustration of the effect is obtained by loading a soda-lime glass plate with a small (1mm diam.) spherical indenter: at comparatively low load the contact is elastic, and the only fracture is that of cone cracking, whereas at higher load some plasticity develops beneath the penetrating sphere, and lateral venting becomes evident in the unloaded plate.[1] A related effect was reported by Culf[7], who observed otherwise regular cone cracks in glass to deflect upward ("hat brim" effect) upon sudden release of the indenter load. Culf also observed considerable residual stress birefringence in association with this phenomenon, over distances large compared with the scale of the deformation zone itself. That residual stresses exist about hardness impressions in most brittle materials has been amply demonstrated by a number of strain-sensitive techniques[8]. That these stresses can also be moderately long-range in nature is seen most clearly in the distances over which relaxation by plastic flow (e.g. dislocation loop punching) occurs in annealing experiments[9]. Neither the existence nor the intensity of the residual elastic fields should come as any surprise, for the stress levels achieved beneath the indenter in hardness tests on highly brittle solids tend to be of the order of the intrinsic bond strength of the structure[10, 11], and the relief of these high stresses would ideally require the impressed region to restore completely to its original unstrained state.

These observations, coupled with a reexamination of the Boussinesq field, provide us with a working model upon which to base an analysis of lateral vent formation. We note that the lateral vents extend in all cases on surfaces closely delineated by families of σ_{11} and σ_{22} trajectories in Fig. 2 (although the paths are modified somewhat by the deformation zone itself, and by free surfaces, including any preexisting median vents or cone cracks); it is as if the applied load were actually reversed upon indenter withdrawal, so that the σ_{33} stress normal to the lateral vent becomes the dominant component of tension in the filed. Of course, it is physically meaningless to associate a reversed applied load with a surface in the unloaded state, but an effectively similar net result may obtain if the deformation zone were to act as a center of contraction with respect to the surrounding elastic matrix. This effect is depicted schematically in Fig. 3. The distribution of stresses at the zone boundary must inevitably depend strongly on the nature of the irreversible deformation (which itself remains an issue of some controversy[11, 12]). Nevertheless, one can proceed by making reasonable assumptions as to this distribution (e.g. that the tractions are of constant magnitude, and are directed such that the net force is zero), and evaluate the residual field in the matrix by taking expressions for the stresses due to elemental point forces (e.g. Mindlin[13]) and integrating around the boundary. One may then construct a stress trajectory pattern for the field, in analogy to Fig. 2, and thereby trace out prospective fracture paths from the deformation zone. Full details of such calculations will be discussed elsewhere; we simply report here that the predicted paths do indeed curve toward the specimen surface in essentially the manner shown in Fig. 1.

The scope of the present model extends well beyond the establishment of a suitable basis for evaluating an "index of brittleness" in standard hardness testing[14]. It provides physical insight into a number of seemingly unrelated phenomena in brittle solids:

(i) Strength degradation. Surface damage introduced into a brittle surface as a result of contact (either static or impact) with hard particles constitutes a potential source of weakness. The mechanics of the damage process may be conveniently simulated in a simple indentation test[15].

(ii) Glass cutting. A glass cutter's wheel is designed to produce a continuous "trailing" median vent as a linear starting crack for subsequent plate fracture in flexure. However, lateral venting invariably occurs in the wake of the moving "indenter", thereby damaging the edges of the final cut. Clearly, the need here is for a means of suppressing the chipping mode.

(iii) Surface removal processes. Individual chipping events in the machining, drilling, grinding, abrasion, erosion and wear of brittle surfaces in general (e.g. ceramics, gemstones, rocks) are of the type depicted in Fig. 1[1]. By summing over an appropriate distribution of such microscopic events, it should be possible to describe macroscopic surface removal parameters at a fundamental level.

(iv) Geophysical impact phenomena. Meteorite-induced craters ranging in scale from geological land masses[16] to lunar fines[17] bear a resemblance to the damage pattern in Fig. 1 which can only be described as striking. While thermal and stress-wave effects associated with the high-velocity impacts are undoubtedly important factors in these cases[18], the possible role of residual stresses about the central "deformation zone" in determining crater morphology may warrant further attention.

B. R. Lawn

Institute for Materials Research
National Bureau of Standards
Washington, D. C. 20234
U. S. A.

M. V. Swain

Martin Marietta Laboratories
1450 South Rolling Road
Baltimore, Md. 21227
U. S. A.

K. Phillips

Division of Materials Science
University of Sussex
Falmer, Sussex BN1 9QT
England

References

1. Lawn, B. R. and Wilshaw, T. R., J. Mater. Sci., in the press.
2. Lawn, B. R. and Swain, M. V., J. Mater. Sci., in the press.
3. Boussinesq, J., Application des Potentiels a l'Etude de l'Equilibre et du Mouvement des Solides Elastiques, (Gauthier-Villars, Paris, 1885). Discussed in Timoshenko, S. P. and Goodier, J. N., Theory of Elasticity (McGraw-Hill, New York, 1970), pp. 398-402.
4. Griffith, A. A., Phil. Trans. Roy. Soc. Lond., A211, 163 (1920).
5. Hertz, H., J. Reine Angew. Math., 92, 156 (1881); Verhandlungen des Vereins zur Beforderung des Gewerbe Fleisses, 61, 449 (1882). Reprinted in English, in Hertz's Miscellaneous Papers (Macmillian, London, 1896), Chs. 5, 6.
6. Frank, F. C. and Lawn, B. R., Proc. Roy. Soc. Lond., A299, 291 (1967).
7. Culf, C. J., J. Soc. Glass.Tech., 41, 157 (1957).
8. Hockey, B. J., in The Science of Hardness Testing and its Research Applications, Symposium Proceedings, Eds. Westbrook, J. H. and Conrad, H. (American Society for Metals, Metals Park, 1973), Ch. 3.
9. Wagatsume, R., Sumino, K., Uchida, W. and Yamamoto, S. J. Appl. Phys., 42, 222 (1971).
10. Kelly, A., Strong Solids (Clarendon, Oxford, 1966).
11. Hill, M. J. and Rowcliffe, D. J., J. Mater. Sci., in the press.
12. Ernsberger, F. M., Ann. Rev. Mat. Sci., 2, 529 (1972).
13. Mindlin, R. D., Physics, 7, 195 (1936).
14. Westbrook, J. H., in The Science of Hardness Testing and its Research Applications, Symposium Proceedings, Eds. Westbrook, J. H. and Conrad, H. (American Society for Metals, Metals Park, 1973), pp. 491-494.

15. Evans, A. G., J. Amer. Ceram. Soc., 56, 405 (1973).

16. Nadai, A., Theory of Flow and Fracture of Solids (McGraw-Hill, New York, 1963), pp. 247-249.

17. Carter, J. L. and MacGregor, I. D., Proc. Apollo 11 Lunar Sci. Conf., 1, 247 (1970).

18. Vedder, J. F. and Mandeville, J.-C., J. Geophys. Res., 79, 3247 (1974).

Figure Captions

1. Fracture geometry beneath sharp indenter. Central deformation zone shown as dark region, median vent cracks as broken lines, lateral vent cracks as heavy lines. (a) Section view schematic, (b) plan view schematic, (c) surface view of fused silica indented with sharp, irregular particle (scanning electron micrograph, field width 3mm).
2. Stress trajectories (curves whose tangent indicates direction of principal stress) for Boussinesq field, showing half-surface view (top) and section view (bottom). Cone cracks initiate from incipient surface flaws and propagate everwhere orthogonally to σ_{11} (tensile outside contact area), median vents initiate from central deformation zone and propagate orthogonally to σ_{22} (tensile below contact zone), lateral vents initiate from deformation zone and propagate nearly orthogonally to σ_{33} (compressive everywhere, but tensile if applied load reversed).
3. Schematic representation of distribution of mismatch tractions at boundary between central deformation zone and surrounding elastic matrix, at indenter withdrawal.

(a)

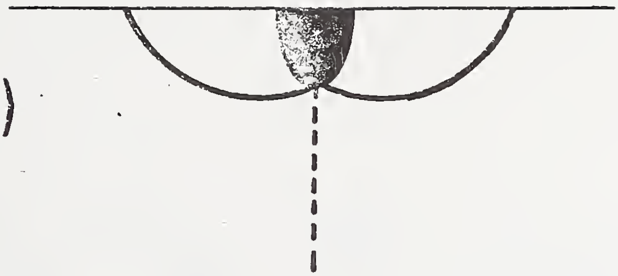

(b)

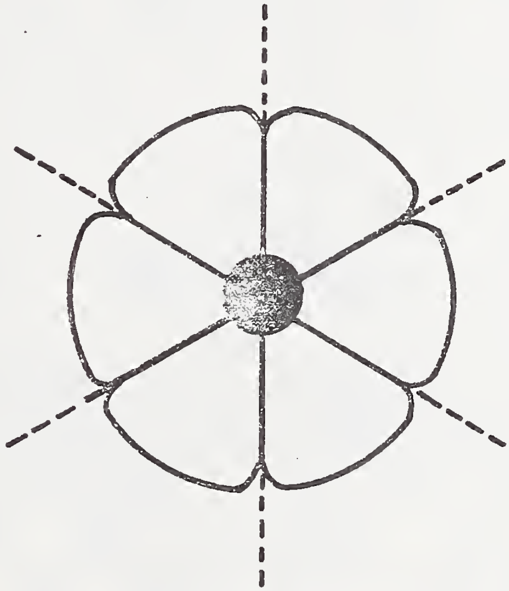

(c)

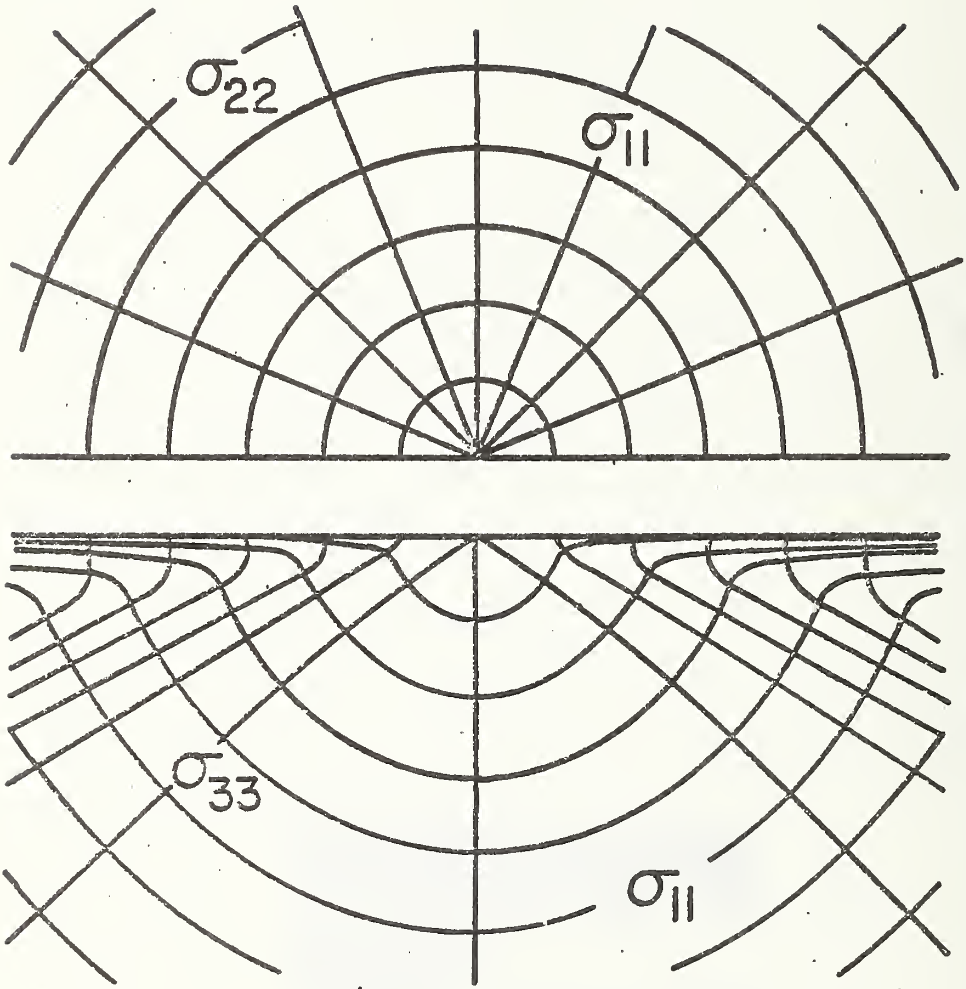
σ_{22}
σ_{11}
σ_{33}
σ_{11}

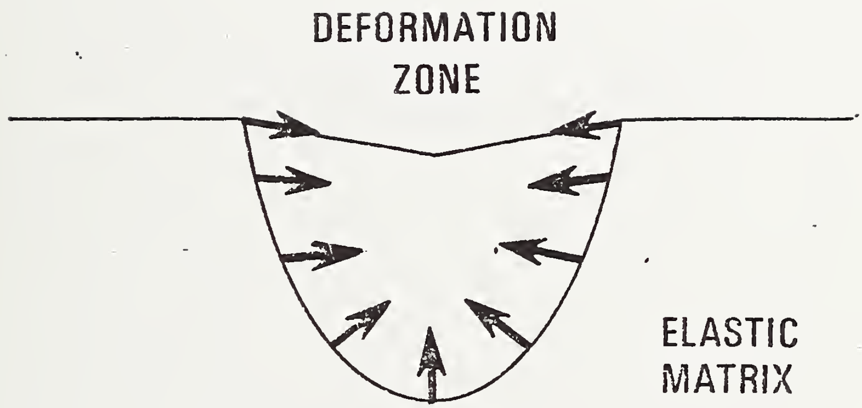
DEFORMATION
ZONE
ELASTIC
MATRIX

II. A Model for the Wear of Brittle Solids Under Fixed Abrasive Conditions

Other than that the wear *mechanism* involves some microfracturing, and the wear *rate* is remarkably high, relatively little is known about the abrasion of highly brittle solids[1,2]; this despite intense current interest in the machining and finishing of brittle surfaces within the ceramics engineering industry[3]. However, with the advent of "indentation fracture mechanics" a new approach has become available for investigating a wide range of small-scale cracking phenomena[4]. The purpose of the present note is to use this approach to construct an explicit model of the wear process in brittle solids, for the simple case of a "fixed" abrasive medium ("two-body" process) in which the grit particles are "ideally sharp."

A schematic representation of the wear mechanism is given in Figure 1. Macroscopically, one measures the wear rate $\dot{V} = dV/dt$ (V = volume removed) appropriate to a specified total load P and velocity v_o for the abrasive medium relative to the specimen. Microscopically, attention focusses on the individual chip-removal mechanism, characterized by an "indenter" load P_i and velocity v_o (all "indenters" traverse the specimen with the same velocity in the two-body configuration). The idea is to start with a mechanical description of the removal process for the i th indenter, and thence to sum over all such i events to predict the macroscopic behavior.

To this end we resort to observations in "model" brittle solids (notably glass) of the fracture patterns beneath standard sharp indenters (e.g. cones, pyramids)[5,6], to build up the following picture. We consider the sliding particle i to produce a "plastic" deformation track of width $2a_i$. Then, for geometrically similar impressions, the mean indentation pressure at any instant of contact may be identified with the material hardness[7],

$$p_i = P_i/\alpha\pi a_i^2 \approx H, \tag{1}$$

where α is a factor determined by indenter geometry. Upon unloading, residual stresses, associated with incompatibility between deformation zone and surrounding elastic matrix, initiate and propagate lateral, chip-forming cracks (so-called "lateral vents"; other cracks form on loading, but these extend straight downward, and play only a secondary role in chipping). In this view, the size of the prospective chip is determined by the configuration of the hardness impression, so the chip area may be written

$$A_i = \eta\, a_i^2, \tag{2}$$

where η is a linear scaling factor. The volume of material removed by the indenting particle in traversing through a distance $\Delta\ell$ in an interval of time Δt is $\Delta V_i = A_i \Delta\ell$, whence, from (1) and (2),

$$\dot{V}_i = \Delta V_i/\Delta t = A_i \Delta\ell/\Delta t = (\eta v_o/\alpha\pi H) P_i. \tag{3}$$

A straightforward summation operation now gives the macroscopic wear rate;

$$\dot{V} = \sum_{i=1}^{N} \dot{V}_i = (\eta v_o/\alpha\pi H) \sum_{i=1}^{N} P_i = \eta v_o P/\alpha\pi H. \tag{4}$$

This equation may be rearranged,

$$\dot{V}/v_o P = \eta/\alpha\pi H, \tag{5}$$

such that the left and right sides conveniently represent macroscopic and microscopic parameters respectively.* It would thus appear possible to predetermine the abrasive wear rate of brittle ceramics simply from quantities measured in standard hardness testing procedures.

Some data from soda-lime glass illustrate the principle. Taking $H \approx 1.0 \times 10^{10}$ Nm^{-2} ("dynamic" hardness)[8], $\alpha \approx 1$ (conical particles), $\eta \approx 1$, we predict $\eta/\alpha\pi H \approx 3 \times 10^{-11}$ m^2 N^{-1} as the wear rate. This compares with $\dot{V}/v_o P \approx 1 \times 10^{-11}$ m^2 N^{-1} measured under test conditions in which chipping is pronounced (namely, spherical specimens on an alumina grinding block pre-ground with 45μm diamond paste, decyl alcohol environment, at P = 10 N, v_o = 1 ms^{-1})[9].

There are some interesting implications associated with the present model:

(i) The calculated wear rate is independent of the (apparent) area of contact between work tool and specimen, and also of the number and size of indenting particles. Thus, all arbitrariness and complication of a statistical analysis is avoided. Physically, this

---

*A term equivalent to that on the left of (5), $\Delta V/P\Delta \ell$, is often used as an alternative expression of the macroscopic wear rate.

arises because of the essential "linearity" of the fixed-abrasive wear mechanism: the chip volume is proportional to the load on the indenting particle, so that the total volume removed does not depend on the way in which the total load is distributed.

(ii) The analysis tacitly assumes that the intensity of the residual stress field about the deformation track is sufficiently high to drive the chip-forming cracks to the surface. The indication from indentation fracture mechanics studies[10] is that the extent of micro-cracking relative to the size of the deformation zone diminishes with decreasing load. Thus we might anticipate a brittle-to-ductile, chipping-to-ploughing transition in wear mechanism at low abrasion loads, small particle sizes, with an attendant fall in wear rate to a value more typical of non-brittle solids[1]. Again, it has been assumed that geometrical similarity is preserved in the indentation fracture process. In practice, initially sharp particles tend to become "blunt" (either by fragmentation or by clogging with debris), and intersections tend to occur between neighboring tracks, as abrasion proceeds; these effects will further reduce the wear rate.

(iii) Most significantly, the wear rate under ideal chipping conditions is uniquely determined by the material <u>hardness</u>; by controlling the <u>scale</u> of the crack pattern behind the indenting particle, the "plasticity" properties of the material assume a key role in the abrasion process. However, hardness is a rate-dependent quantity which can change markedly with the conditions of testing, e.g. environment, load rate (sliding velocity), etc.[8,11] This bears strongly on the correlations between a wide range of chemo-mechanical properties (e.g. machining, drilling, grinding) and the hardness of brittle materials reported by Westwood and co-workers[12]. While the present model may provide a sound basis for interpreting chemo-mechanical phenomena, it needs to be emphasised that correlations of this type can be truly meaningful only if the hardness values are measured under conditions pertinent to the macroscopic situation.

Acknowledgements

The author is indebted to S. M. Wiederhorn and H. H. Johnson for discussions on this work. The sponsorship by the Office of Naval Research, under Contract No. NR-032-535, is acknowledged.

Figure Captions

1. Cross-sectional views of "fixed" abrasion process. (a) Macroscopic view: total load P bears on specimen via abrasive grit particles bonded to tool. (b) Microscopic view: i th particle experiences load P_i, and leaves in its wake a deformation track, width $2a_i$, from which "lateral vents" propagate to form chip, section area A_i. All particles translate across specimen surface with velocity v_o.

References

1. E. Rabinowicz, Friction and Wear of Materials, Wiley, New York, 1965, Ch. 7.

2. M. M. Kruschov, Wear, 28 (1974) 69.

3. The Science of Ceramic Machining and Surface Finishing, Symposium Proceedings, N. B. S. Special Publ. 348, 1972.

4. B. R. Lawn and T. R. Wilshaw, J. Mater. Sci. (in press).

5. B. R. Lawn and M. V. Swain, J. Mater. Sci. (in press).

6. B. R. Lawn, M. V. Swain and K. Phillips, to be published.

7. D. Tabor, The Hardness of Metals, Clarendon, Oxford, 1951, Ch. 1.

8. S. P. Gunasekera and D. G. Holloway, Phys. and Chem. Glasses, 14 (1973) 45.

9. S. M. Wiederhorn and D. E. Roberts, Wear, 32 (1975) 51.

10. B. R. Lawn and E. R. Fuller, to be published.

11. R. E. Hanneman and J. H. Westbrook, Phil. Mag. 18 (1968) 73.

12. A. R. C. Westwood and N. H. Macmillan, The Science of Hardness Testing and its Research Applications, Symposium Proceedings, American Society for Metals, 1973, Ch. 28.

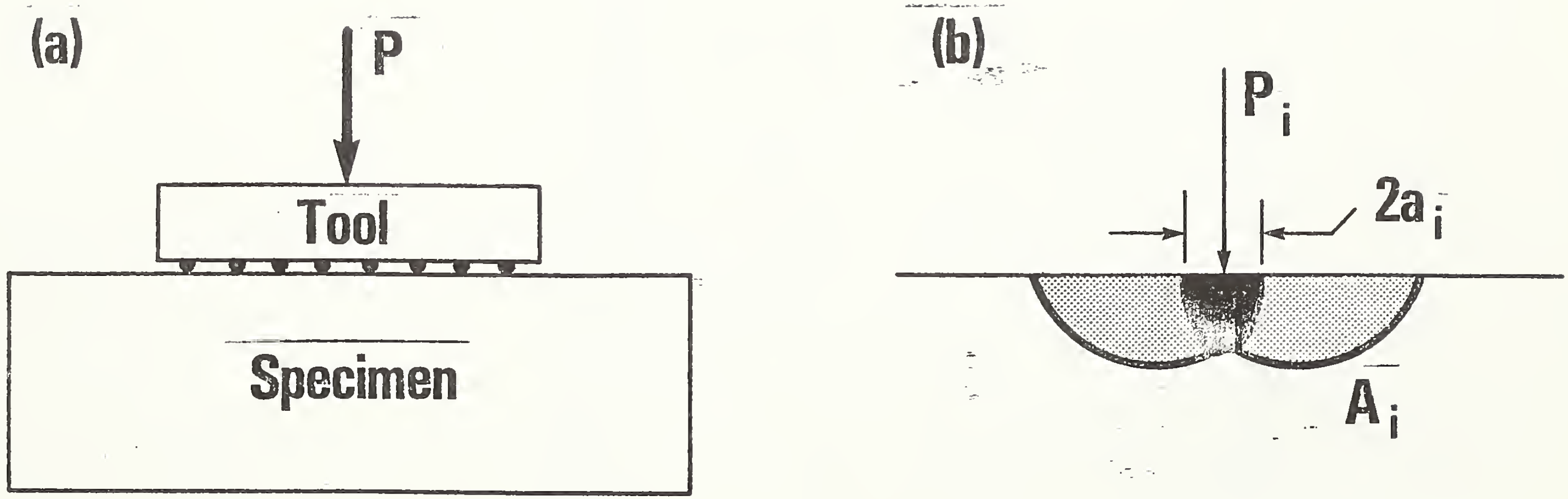
(a)
P
Tool
Specimen
(b)
P_i
$2a_i$
A_i

A MODEL FOR THE WEAR OF BRITTLE SOLIDS

UNDER FIXED ABRASIVE CONDITIONS

B. R. Lawn*

Institute for Materials Research, National Bureau of Standards, Washington, D. C. 20234, U.S.A.

*On study leave, from School of Physics, University of New South Wales, Kensington, N. S. W. 2033, Australia

Other than that the wear <u>mechanism</u> involves some microfracturing, and the wear <u>rate</u> is remarkably high, relatively little is known about the abrasion of highly brittle solids[1,2]; this despite intense current interest in the machining and finishing of brittle surfaces within the ceramics engineering industry[3]. However, with the advent of "indentation fracture mechanics" a new approach has become available for investigating a wide range of small-scale cracking phenomena[4]. The purpose of the present note is to use this approach to construct an explicit model of the wear process in brittle solids, for the simple case of a "fixed" abrasive medium ("two-body" process) in which the grit particles are "ideally sharp."

A schematic representation of the wear mechanism is given in Figure 1. Macroscopically, one measures the wear rate $\dot{V} = dV/dt$ (V = volume removed) appropriate to a specified total load P and velocity v_o for the abrasive medium relative to the specimen. Microscopically, attention focusses on the individual chip-removal mechanism, characterized by an "indenter" load P_i and velocity v_o (all "indenters" traverse the specimen with the same velocity in the two-body configuration). The idea is to start with a mechanical description of the removal process for the i th indenter, and thence to sum over all such i events to predict the macroscopic behavior.

To this end we resort to observations in "model" brittle solids (notably glass) of the fracture patterns beneath standard sharp indenters (e.g. cones, pyramids)[5,6], to build up the following picture. We consider the sliding particle i to produce a "plastic" deformation track of width $2a_i$. Then, for geometrically similar impressions, the mean indentation pressure at any instant of contact may be identified with the material hardness[7],

$$p_i = P_i/\alpha\pi a_i^2 \approx H, \tag{1}$$

where α is a factor determined by indenter geometry. Upon unloading, residual stresses, associated with incompatibility between deformation zone and surrounding elastic matrix, initiate and propagate lateral, chip-forming cracks (so-called "lateral vents"; other cracks form on loading, but these extend straight downward, and play only a secondary role in chipping). In this view, the size of the prospective chip is determined by the configuration of the hardness impression, so the chip area may be written

$$A_i = \eta\, a_i^2, \tag{2}$$

where η is a linear scaling factor. The volume of material removed by the indenting particle in traversing through a distance $\Delta \ell$ in an interval of time Δt is $\Delta V_i = A_i \Delta \ell$, whence, from (1) and (2),

$$\dot{V}_i = \Delta V_i/\Delta t = A_i \Delta \ell/\Delta t = (\eta v_o/\alpha\pi H)P_i. \tag{3}$$

A straightforward summation operation now gives the macroscopic wear rate;

$$\dot{V} = \sum_{i=1}^{N} \dot{V}_i = (\eta v_o/\alpha\pi H) \sum_{i=1}^{N} P_i = \eta v_o P/\alpha\pi H. \tag{4}$$

This equation may be rearranged,

$$\dot{V}/v_o P = \eta/\alpha\pi H, \tag{5}$$

such that the left and right sides conveniently represent macroscopic and microscopic parameters respectively.* It would thus appear possible to predetermine the abrasive wear rate of brittle ceramics simply from quantities measured in standard hardness testing procedures.

Some data from soda-lime glass illustrate the principle. Taking $H \approx 1.0 \times 10^{10}$ Nm^{-2} ("dynamic" hardness)[8], $\alpha \approx 1$ (conical particles), $\eta \approx 1$, we predict $\eta/\alpha\pi H \approx 3 \times 10^{-11}$ m^2 N^{-1} as the wear rate. This compares with $\dot{V}/v_o P \approx 1 \times 10^{-11}$ m^2 N^{-1} measured under test conditions in which chipping is pronounced (namely, spherical specimens on an alumina grinding block pre-ground with 45μm diamond paste, decyl alcohol environment, at $P = 10$ N, $v_o = 1$ ms^{-1})[9].

There are some interesting implications associated with the present model:

(i) The calculated wear rate is independent of the (apparent) area of contact between work tool and specimen, and also of the number and size of indenting particles. Thus, all arbitrariness and complication of a statistical analysis is avoided. Physically, this

---

*A term equivalent to that on the left of (5), $\Delta V/P\Delta \ell$, is often used as an alternative expression of the macroscopic wear rate.

arises because of the essential "linearity" of the fixed-abrasive wear mechanism: the chip volume is proportional to the load on the indenting particle, so that the total volume removed does not depend on the way in which the total load is distributed.

(ii) The analysis tacitly assumes that the intensity of the residual stress field about the deformation track is sufficiently high to drive the chip-forming cracks to the surface. The indication from indentation fracture mechanics studies[10] is that the extent of micro-cracking relative to the size of the deformation zone diminishes with decreasing load. Thus we might anticipate a brittle-to-ductile, chipping-to-ploughing transition in wear mechanism at low abrasion loads, small particle sizes, with an attendant fall in wear rate to a value more typical of non-brittle solids[1]. Again, it has been assumed that geometrical similarity is preserved in the indentation fracture process. In practice, initially sharp particles tend to become "blunt" (either by fragmentation or by clogging with debris), and intersections tend to occur between neighboring tracks, as abrasion proceeds; these effects will further reduce the wear rate.

(iii) Most significantly, the wear rate under ideal chipping conditions is uniquely determined by the material <u>hardness</u>; by controlling the <u>scale</u> of the crack pattern behind the indenting particle, the "plasticity" properties of the material assume a key role in the abrasion process. However, hardness is a rate-dependent quantity which can change markedly with the conditions of testing, e.g. environment, load rate (sliding velocity), etc.[8,11] This bears strongly on the correlations between a wide range of chemo-mechanical properties (e.g. machining, drilling, grinding) and the hardness of brittle materials reported by Westwood and co-workers[12]. While the present model may provide a sound basis for interpreting chemo-mechanical phenomena, it needs to be emphasised that correlations of this type can be truly meaningful only if the hardness values are measured under conditions pertinent to the macroscopic situation.

Acknowledgements

The author is indebted to S. M. Wiederhorn and H. H. Johnson for discussions on this work. The sponsorship by the Office of Naval Research, under Contract No. NR-032-535, is acknowledged.

References

1. E. Rabinowicz, Friction and Wear of Materials, Wiley, New York, 1965, Ch. 7.

2. M. M. Kruschov, Wear, 28 (1974) 69.

3. The Science of Ceramic Machining and Surface Finishing, Symposium Proceedings, N. B. S. Special Publ. 348, 1972.

4. B. R. Lawn and T. R. Wilshaw, J. Mater. Sci. (in press).

5. B. R. Lawn and M. V. Swain, J. Mater. Sci. (in press).

6. B. R. Lawn, M. V. Swain and K. Phillips, to be published.

7. D. Tabor, The Hardness of Metals, Clarendon, Oxford, 1951, Ch. 1.

8. S. P. Gunasekera and D. G. Holloway, Phys. and Chem. Glasses, 14 (1973) 45.

9. S. M. Wiederhorn and D. E. Roberts, Wear, 32 (1975) 51.

10. B. R. Lawn and E. R. Fuller, to be published.

11. R. E. Hanneman and J. H. Westbrook, Phil. Mag. 18 (1968) 73.

12. A. R. C. Westwood and N. H. Macmillan, The Science of Hardness Testing and its Research Applications, Symposium Proceedings, American Society for Metals, 1973, Ch. 28.

Figure Captions

1. Cross-sectional views of "fixed" abrasion process. (a) Macroscopic view: total load P bears on specimen via abrasive grit particles bonded to tool. (b) Microscopic view: i th particle experiences load P_i, and leaves in its wake a deformation track, width $2a_i$, from which "lateral vents" propagate to form chip, section area A_i. All particles translate across specimen surface with velocity v_o.

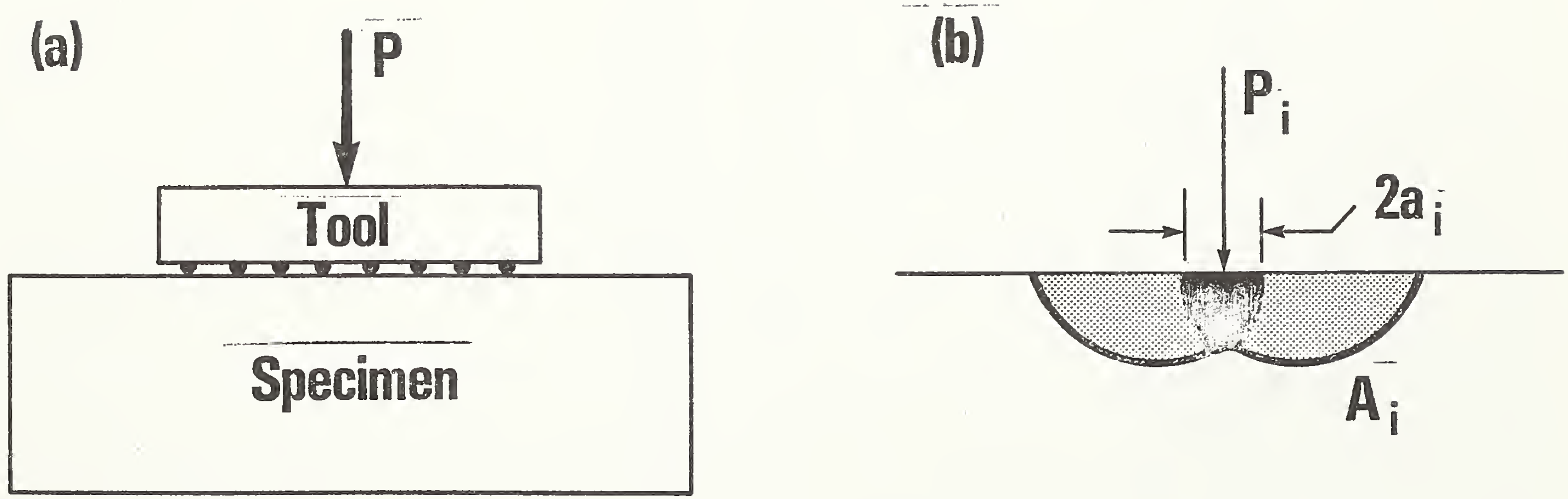
(a)
P
Tool
Specimen
(b)
P_i
$2a_i$
A_i

On the Mode of Chipping Fracture in Brittle Solids

Chipping processes in brittle solids, despite their unquestionable relevance to a diversity of technologies from ceramics finishing to geological engineering, are not well understood at the fundamental level. Some recent studies of microfracture patterns beneath standard hardness indenters do, however, shed some light on the problem[1, 2]. Essentially, the picture which emerges is that depicted in Fig. 1: (i) Upon loading the indenter a confined zone of irreversible (plastic) deformation forms about any sharp points or corners (thereby accounting for the residual hardness impression), from which "median vent" cracks first initiate and subsequently propagate radially outward along suitable planes of symmetry (e.g. as defined by the diagonals of a pyramid indenter, or by preferred cleavage planes) containing the contact axis; (ii) Upon unloading the indenter the median vents close up, but, just prior to complete removal, "lateral vent" cracks initiate and extend laterally from the deformation zone toward the specimen surface. Of the two types of cracking it is clearly the second which relates more directly to brittle chipping.

Yet up till now a detailed fracture mechanics analysis has been attempted only for the median vent system. This system is relatively well defined, since the indentation stress field, which uniquely determines the extent of crack growth[1], can reasonably be represented in terms of the classical Boussinesq field for normal point loading[2, 3]. On the basis of the fundamental Griffith energy-balance condition for fracture[4] it may readily be argued that brittle cracks will generally tend to follow trajectories of the lesser principal stresses within the indentation field, such that the path maintains near-orthogonality to a component of major tension: the best-studied illustration of this principle is the Hertzian cone crack [5, 6], which, in the absence of any deformation-induced nucleation center, initiates from an incipient surface flaw and flares downward into the specimen. In the scheme of Fig. 2, in which the principal stresses are defined such that $\sigma_{11} \geq \sigma_{22} \geq \sigma_{33}$ (positive values denoting tension) nearly everywhere, median vent geometry may be specified in terms of families of σ_{11} and σ_{33} trajectories, cone crack geometry in terms of families of σ_{22} and σ_{33} trajectories.

The conditions under which the lateral vents form are, unfortunately, less easily modelled. Since the lateral system operates only as the indenter is withdrawn from the specimen surface it is evident that the driving force for propagation must originate from some residual stress field associated with the irreversible deformation zone. This conclusion is substantiated by microscopic investigation of the damage patterns as a function of indenter geometry (e.g. "sharp" or "blunt"): in general, the extent of lateral venting is found to increase markedly with expanding zone size. A graphic illustration of the effect is obtained by loading a soda-lime glass plate with a small (1mm diam.) spherical indenter: at comparatively low load the contact is elastic, and the only fracture is that of cone cracking, whereas at higher load some plasticity develops beneath the penetrating sphere, and lateral venting begins to extablish itself[1]. A manifestation of this behavior was reported by Culf[7], who observed otherwise regular cone cracks in glass to deflect upward ("hat brim" effect) upon sudden release of the indenter load. Culf also observed considerable residual stress birefringence in association with this phenomenon, over distances large compared with the scale of the deformation zone itself. That residual stresses exist about hardness impressions in most brittle materials has been amply demonstrated by a number of strain-sensitive techniques[8]. That these stresses can also be moderately long-range in nature is seen most clearly in the distances over which relaxation by plastic flow (e.g. dislocation loop punching) occurs in annealing experiments[9]. Neither the existence nor the intensity of the residual elastic fields should come as any surprise, for the stress levels achieved beneath the indenter in hardness tests on highly brittle solids tend to be of the order of the intrinsic bond strength of the structure[10, 11], and the relief of these high stresses would ideally require the impressed region to restore completely to its original unstrained state.

These observations, coupled with a reexamination of the Boussinesq field, provide us with the basis for an analysis of lateral vent geometry. We note that the lateral vents extend in all cases on surfaces closely delineated by families of σ_{11} and σ_{22} trajectories in Fig. 2 (although the paths are modified somewhat by the deformation zone itself, and by free surfaces, including any preexisting median vents or cone cracks); it is as if the applied load were actually <u>reversed</u> upon indenter withdrawal, so that the σ_{33} stress normal to the lateral vent becomes the dominant component of tension in the filed. Of course, it is physically meaningless to associate a reversed applied load with a surface in the unloaded state, but an effectively similar net result may obtain if the deformation zone were to act as a center of contraction with respect to the surrounding elastic matrix. This is depicted schematically in Fig. 3. The distribution of stresses at the zone boundary must inevitably depend strongly on the nature of the irreversible deformation, which itself remains an issue of some controversy[11, 12]. Nevertheless, one can proceed by making reasonable assumptions as to this distribution (e.g. that the tractions are of constant magnitude, and are directed such that the net force is zero), and evaluate the residual field in the matrix by taking expressions for the stresses due to elemental point forces (e.g. Mindlin[13]) and integrating around the boundary. One may then construct a stress trajectory pattern for the field, in analogy to Fig. 2, and thereby trace out probable fracture paths from the deformation zone. Full details of such calculations will be discussed elsewhere; we simply report here that the predicted paths do indeed curve toward the specimen surface in essentially the manner shown in Fig. 1.

The scope of the present model extends well beyond the establishment of a suitable basis for evaluating an "index of brittleness" in standard harndess testing[14]. It provides physical insight into a number of seemingly unrelated phenomena in brittle solids:

(i) Strength degradation. Surface damage introduced into a brittle surface as a result of contact (either static or impact) with hard particles constitutes a potential source of weakness. The mechanics of the damage process may be conveniently simulated in a simple indentation test[15].

(ii) Glass cutting. A glass cutter's wheel is designed to produce a continuous "trailing" median vent as a linear starting crack for subsequent plate fracture in flexure. However, lateral venting invariably occurs in the wake of the moving "indenter", thereby damaging the edges of the final cut. Clearly, the objective here is to find a way of suppressing the chipping mode.

(iii) Surface removal processes. Individual chipping events in the machining, drilling, grinding, abrasion, erosion and wear of brittle surfaces in general (e.g. ceramics, gemstones, rocks) are of the type depicted in Fig. 1[1]. By summing over an appropriate distribution of such microscopic events it should be possible to describe macroscopic surface removal parameters at a fundamental level.

(iv) Geophysical impact phenomena. Meteorite-induced craters ranging in scale from geological land masses[16] to lunar fines[17] bear a resemblance to the damage pattern in Fig. 1 which can only be described as striking. While thermal and stress-wave effects associated with the high-velocity impacts are undoubtedly important factors in these cases[18], the possible role of residual stresses about the central "deformation zone" in determining crater morphology may warrant further attention.

B. R. Lawn

Institute for Materials Research
National Bureau of Standards
Washington, D. C. 20234
U. S. A.

M. V. Swain

Martin Marietta Laboratories
1450 South Rolling Road
Baltimore, Md. 21227
U. S. A.

K. Phillips

Division of Materials Science
University of Sussex
Falmer, Sussex BN1 9QT
England

References

1. Lawn, B. R. and Wilshaw, T. R., J. Mater. Sci., in the press.
2. Lawn, B. R. and Swain, M. V., J. Mater. Sci., in the press.
3. Boussinesq, J., Application des Potentiels a l'Etude de l'Equilibre et du Mouvement des Solides Elastiques, (Gauthier-Villars, Paris, 1885). Discussed in Timoshenko, S. P. and Goodier, J. N., Theory of Elasticity (McGraw-Hill, New York, 1970), pp. 398-402.
4. Griffith, A. A., Phil. Trans. Roy. Soc. Lond., A211, 163 (1920).
5. Hertz, H., J. Reine Angew. Math., 92, 156 (1881); Verhandlungen des Vereins zur Beforderung des Gewerbe Fleisses, 61, 449 (1882). Reprinted in English, in Hertz's Miscellaneous Papers (Macmillian, London, 1896), Chs. 5, 6.
6. Frank, F. C. and Lawn, B. R., Proc. Roy. Soc. Lond., A299, 291 (1967).
7. Culf, C. J., J. Soc. Glass.Tech., 41, 157 (1957).
8. Hockey, B. J., in The Science of Hardness Testing and its Research Applications, Symposium Proceedings, Eds. Westbrook, J. H. and Conrad, H. (American Society for Metals, Metals Park, 1973), Ch. 3.
9. Wagatsume, R., Sumino, K., Uchida, W. and Yamamoto, S. J. Appl. Phys., 42, 222 (1971).
10. Kelly, A., Strong Solids (Clarendon, Oxford, 1966).
11. Hill, M. J. and Rowcliffe, D. J., J. Mater. Sci., in the press.
12. Ernsberger, F. M., Ann. Rev. Mat. Sci., 2, 529 (1972).
13. Mindlin, R. D., Physics, 7, 195 (1936).
14. Westbrook, J. H., in The Science of Hardness Testing and its Research Applications, Symposium Proceedings, Eds. Westbrook, J. H. and Conrad, H. (American Society for Metals, Metals Park, 1973), pp. 491-494.

15. Evans, A. G., J. Amer. Ceram. Soc., 56, 405 (1973).

16. Nadai, A., Theory of Flow and Fracture of Solids (McGraw-Hill, New York, 1963), pp. 247-249.

17. Carter, J. L. and MacGregor, I. D., Proc. Apollo 11 Lunar Sci. Conf., 1, 247 (1970).

18. Vedder, J. F. and Mandeville, J.-C., J. Geophys. Res., 79, 3247 (1974).

Figure Captions

1. Fracture geometry beneath sharp indenter. Central deformation zone shown as dark region, median vent cracks as broken lines, lateral vent cracks as heavy lines. (a) Section view schematic, (b) plan view schematic, (c) surface view of fused silica indented with sharp, irregular particle (scanning electron micrograph).
2. Stress trajectories (curves whose tangent indicates direction of principal stress) for Boussinesq field, showing half-surface view (top) and section view (bottom). Cone cracks initiate from incipient surface flaws and propagate everwhere orthogonally to σ_{11} (tensile outside contact area), median vents initiate from central deformation zone and propagate orthogonally to σ_{22} (tensile below contact zone), lateral vents initiate from deformation zone and propagate nearly orthogonally to σ_{33} (compressive everywhere, but tensile if applied load reversed).
3. Schematic representation of distribution of mismatch tractions at boundary between central deformation zone and surrounding elastic matrix, at indenter withdrawal.

(a)

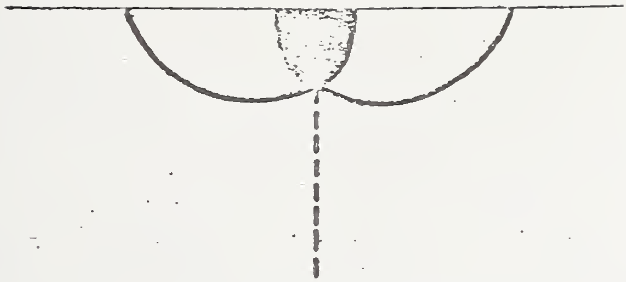

(b)

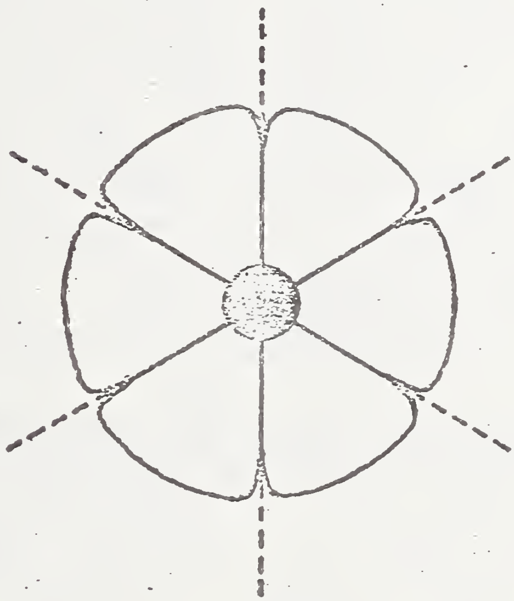

(c)

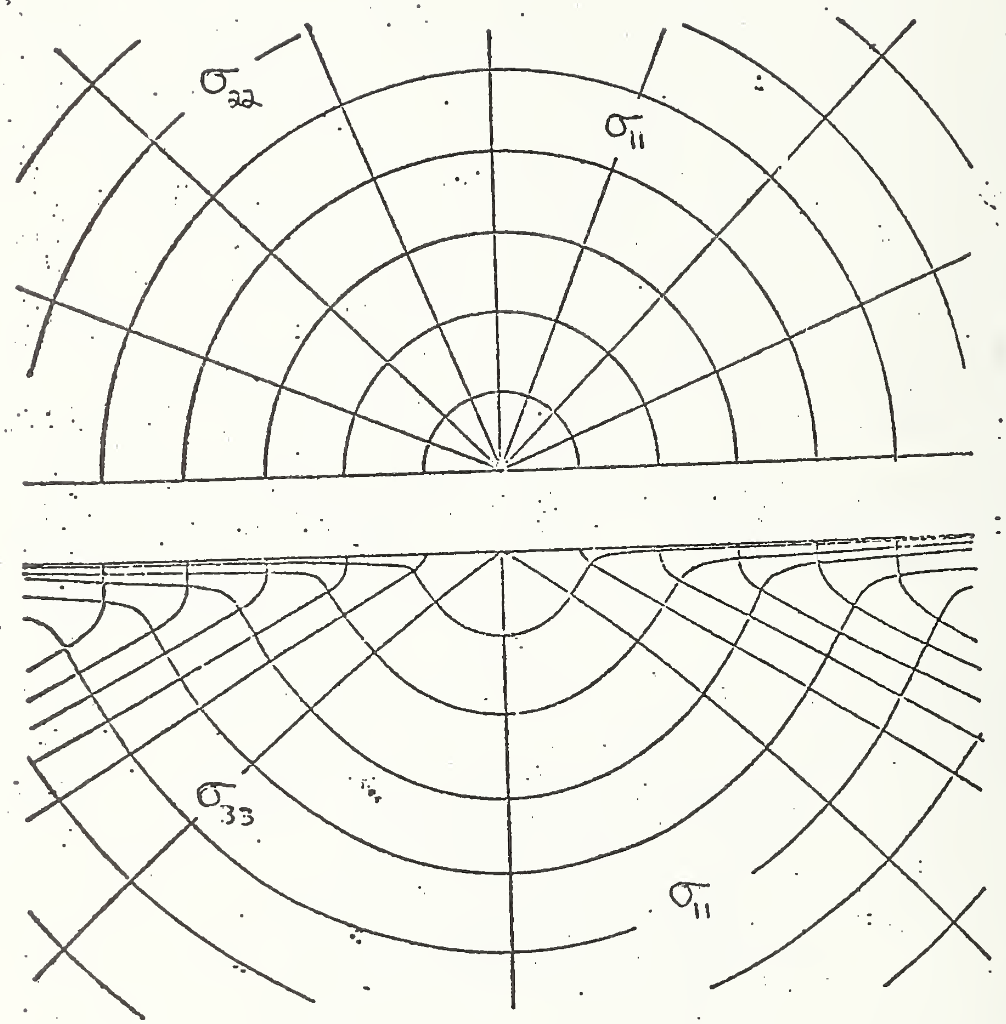

σ_{22}
σ_{11}
σ_{33}
σ_{11}

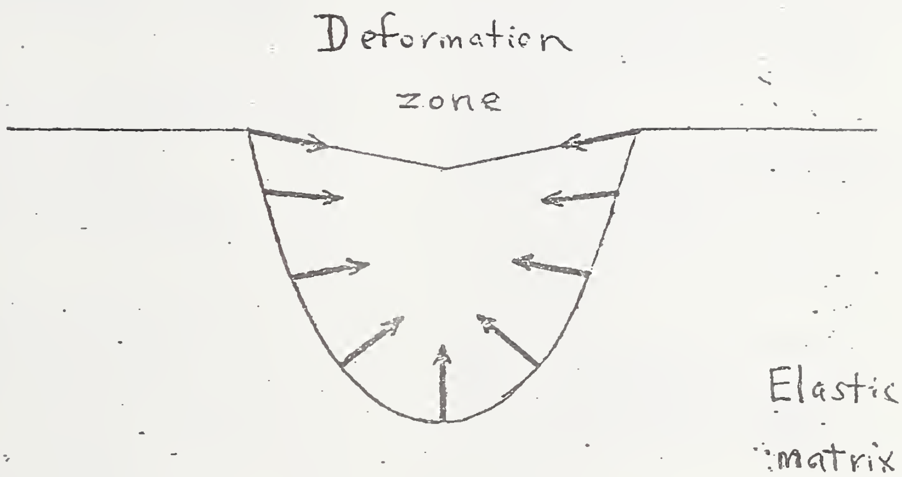
Deformation
zone
Elastic
matrix

DISTRIBUTION LIST

Organization

Office of Naval Research
Department of the Navy
Attn: Code 471
Arlington, Virginia 22217

Director
Office of Naval Research
Branch Office
495 Summer Street
Boston, Massachusetts 02210

Director
Office of Naval Research
New York Area Office
207 West 24th Street
New York, New York 10011

Director
Office of Naval Research
Branch Office
1030 East Green Street
Pasadena, California 91101

Commanding Officer
Naval Weapons Laboratory
Attn: Research Division
Dahlgren, Virginia 22448

Director
Naval Research Laboratory
Attn: Technical Information Officer
Code 2000
Washington, D. C. 20390

Director
Naval Research Laboratory
Attn: Technical Information Officer
Code 2020
Washington, D. C. 20390

Director
Naval Research Laboratory
Attn: Technical Information Officer
Code 6000
Washington, D. C. 20390

Organization

Director
Naval Research Laboratory
Attn: Technical Information Officer
Code 6100
Washington, D. C. 20390

Director
Naval Research Laboratory
Attn: Technical Information Officer
Code 6300
Washington, D. C. 20390

Director
Naval Research Laboratory
Attn: Technical Information Officer
Code 6400
Washington, D. C. 20390

Director
Naval Research Laboratory
Attn: Library
Code 2029 (ONRL)
Washington, D. C. 20390

Commander
Naval Air Systems Command
Department of the Navy
Attn: Code AIR 320A
Washington, D. C. 20360

Commander
Naval Air System Command
Department of the Navy
Attn: Code AIR 5203
Washington, D. C. 20360

Commander
Naval Ordnance Systems Command
Department of the Navy
Attn: Code ORD 033
Washington, D. C. 20360

Commanding Officer
Naval Air Development Center
Aeronautical Materials Div.
Johnsville
Attn: Code MAM
Warminster, Pa. 18974

Commanding Officer
Naval Ordnance Laboratory
Attn: Code 210
White Oak
Silver Spring, Maryland 20910

Commander
Naval Ship Systems Command
Department of the Navy
Attn: Code 0342
Washington, D. C. 20360

Commanding Officer
Naval Civil Engineering Laboratory
Attn: Code L70
Port Hueneme, California 93041

Commander
Naval Ship Engineering Center
Department of the Navy
Attn: Code 6101
Washington, D. C. 20360

Naval Ships R&D Laboratory
Annapolis Division
Attn: Code A800
Annapolis, Maryland 21402

Commanding Officer
Naval Ships R&D Center
Attn: Code 747
Washington, D. C. 20007

Commander Naval Weapons Center
Naval Weapons Center
Attn: Code 5560
China Lake, California 93555

Commander
Naval Underseas Warfare Center
Pasadena, California 92152

Scientific Advisor
Commandant of the Marine Corps
Attn: Code AX
Washington, D. C. 20380

Commanding Officer
Army Research Office, Durham
Box CM, Duke Station
Attn: Metallurgy & Ceramics Div.
Durham, North Carolina 27706

Office of Scientific Research
Department of the Air Force
Attn: Solid State Div. (SRPS)
Washington, D. C. 20333

Defense Documentation Center
Cameron Station
Alexandria, Virginia 22314

National Bureau of Standards
Attn: Metallurgy Division
Washington, D. C. 20234

National Bureau of Standards
Attn: Inorganic Materials Div.
Washington, D. C. 20234

Atomic Energy Commission
Attn: Metals & Materials Branch
Washington, D. C. 20545

Argonne National Laboratory
Metallurgy Division
P. O. Box 299
Lemont, Illinois 60439

Brookhaven National Laboratory
Technical Information Division
Attn: Research Library
Upton, Long Island, New York 11973

Library
Bldg. 50, Room 134
Lawrence Radiation Laboratory
Berkeley, California 94720

Los Alamos Scientific Laboratory
P. O. Box 1663
Attn: Report Librarian
Los Alamos, New Mexico 87544

Commanding Officer
Army Materials and Mechanics
Research Center
Attn: Res. Programs Office (AMXMR-P)
Watertown, Massachusetts 02172

Director
Metals & Ceramics Division
Oak Ridge National Laboratory
P. O. Box X
Oak Ridge, Tennessee 37830

Commanding Officer
Naval Underwater Systems Center
Newport, Rhode Island 02844

Aerospace Research Laboratories
Wright-Patterson AFB
Building 450
Dayton, Ohio 45433

Defense Metals Information Center
Battelle Memorial Institute
505 King Avenue
Columbus, Ohio 43201

Army Electronics Command
Evans Signal Laboratory
Solid State Devices Branch
c/o Senior Navy Liaison Officer
Fort Monmouth, New Jersey 07703

Commanding General
Department of the Army
Frankford Arsenal
Attn: ORDBA-1320, 64-4
Philadelphia, Pennsylvania 19137

Executive Director
Materials Advisory Board
National Academy of Sciences
2101 Constitution Avenue, N. W.
Washington, D. C. 20418

NASA Headquarters
Attn: Code RRM
Washington, D. C. 20546

Air Force Materials Lab
Wright-Patterson AFB
Attn: MAMC
Dayton, Ohio 45433

Air Force Materials Lab
Wright-Patterson AFB
Attn: MAAM
Dayton, Ohio 45433

Deep Submergence Systems Project
Attn: DSSP-00111
Washington, D. C. 20360

Advanced Research Projects Agency
Attn: Director, Materials Science
Washington, D. C. 20301

Department of the Interior
Bureau of Mines
Attn: Science & Engineering Advisor
Washington, D. C. 20240

Defense Ceramics Information Center
Battelle Memorial Institute
505 King Avenue
Columbus, Ohio 43201

National Aeronautics & Space Adm.
Lewis Research Center
Attn: Librarian
21000 Brookpark Rd.
Cleveland, Ohio 44135

Naval Missile Center
Materials Consultant
Code 3312-1
Point Mugu, California 93041

Commanding Officer
Naval Weapons Center Corona Labs.
Corona, California 91720

Commander
Naval Air Test Center
Weapons Systems Test Div. (Code O1A)
Patuxent River, Maryland 20670

Director
Ordnance Research Laboratory
P. O. Box 30
State College, Pennsylvania 16801

Director
Applied Physics Laboratory
1013 Northeast Fortieth St.
Seattle, Washington 98105

Materials Sciences Group
Code S130.1
271 Catalina Boulevard
Navy Electronics Laboratory
San Diego, California 92152

Dr. Waldo K. Lyon
Director, Arctic Submarine Laboratory
Code 90, Building 371
Naval Undersea R&D Center
San Diego, California 92132

Dr. R. Nathan Katz
Ceramics Division
U.S. Army Materials & Mechanics
Research Center
Watertown, Mass. 02172

SUPPLEMENTARY DISTRIBUTION LIST

Professor R. Roy
Materials Research Laboratory
Pennsylvania State University
University Park, Pennsylvania 16802

Professor D. H. Whitmore
Department of Metallurgy
Northwestern University
Evanston, Illinois 60201

Professor J. A. Pask
Department of Mineral Technology
University of California
Berkeley, California 94720

Professor D. Turnbull
Div. of Engineering and Applied Sci.
Harvard University
Pierce Hall
Cambridge, Massachusetts 02100

Dr. T. Vasilos
AVCO Corporation
Research and Advanced Development Div.
201 Lowell St.
Wilmington, Massachusetts 01887

Dr. H. A. Perry
Naval Ordnance Laboratory
Code 230
Silver Spring, Maryland 20910

Dr. Paul Smith
Crystals Branch, Code 6430
Naval Research Laboratory
Washington, D. C. 20390

Dr. A. R. C. Westwood
RIAS Division
Martin-Marietta Corporation
1450 South Rolling Road
Baltimore, Maryland 21227

Dr. W. Haller
Chief, Inorganic Glass Section
National Bureau of Standards
Washington, D. C. 20234

Dr. R. H. Doremus
General Electric Corporation
Metallurgy and Ceramics Lab.
Schenectady, New York 12301

Professor G. R. Miller
Department of Ceramic Engineering
University of Utah
Salt Lake City, Utah 84112

Dr. T. D. Chikalla
Fuels and Matls. Department
Battelle Northwest
P. O. Box 999
Richland, Washington 99352

Mr. I . Berman
Army Materials and Mechanics
Research Center
Watertown, Massachusetts 02171

Dr. F. F. Lange
Westinghouse Electric Corporation
Research Laboratories
Pittsburgh, Pennsylvania 15235

Professor H. A. McKinstry
Pennsylvania State University
Materials Research Laboratory
University Park, Pa. 16802

Professor T. A. Litovitz
Physics Department
Catholic University of America
Washington, D. C. 20017

Dr. R. J. Stokes
Honeywell Corporate Research Center
10701 Lyndale Avenue South
Bloomington, Minnesota 55420

Dr. Harold Liebowitz
Dean of Engineering
George Washington Univeristy
Washington, D. C. 20006

Dr. H. Kirchner
Ceramic Finishing Company
P. O. Box 498
State College, Pennsylvania 16801

Professor A. H. Heuer
Case Western Reserve University
University Circle
Cleveland, Ohio 44106

Dr. D. E. Niesz
Battelle Memorial Institute
505 King Avenue
Columbus, Ohio 43201

Dr. F. A. Kroger
University of Southern California
University Park
Los Angeles, California 90007

Dr. Sheldon M. Wiederhorn
National Bureau of Standards
Inorganic Materials Division
Washington, D. C. 20234

Dr. C. O. Hulse
United Aircraft Research Labs
United Aircraft Corporation
East Hartford, Connecticut 06108

Professor M. H. Manghnani
University of Hawaii
Hawaii Institute of Geophysics
2525 Correa Road
Honolulu, Hawaii 96822

Dr. Stephen Malkin
Department of Mechanical Engineering
University of Texas
Austin, Texas 78712

Prof. H. E. Wilhelm
Department of Mechanical Engineering
Colorado State University
Fort Collins, Colorado 80521

Stanford University
Dept. of Materials Sciences
Stanford, California 94305

Dr. R. K. MacCrone
Department of Materials Engineering
Rensselaer Polytechnic Institute
Troy, New York 12181

Dr. D. C. Mattis
Belfer Graduate School of Science
Yeshiva University
New York, New York 10033

Professor R. B. Williamson
College of Engineering
University of California
Berkeley, California 94720

Professor R.. W. Gould
Department of Metallurgical
and Materials Engineering
College of Engineering
University of Florida
Gainesville, Florida 32601

Professor V. S. Stubican
Department of Materials Science
Ceramic Science Section
Pennsylvania State University
University Park, Pennsylvania 16802

Dr. R. C. Anderson
General Electric Company
Miniature Lamp Department
Nela Park
Cleveland, Ohio 44112

Dr. Bert Zauderer
MHD Program, Advanced Studies
Room L-9513-VFSC
General Electric Company
P. O. Box 8555
Philadelphia, Pennsylvania 19101

Prof. C. F. Fisher, Jr.
Department of Mechanical and Aero-
Space Engineering
University of Tennessee
Knoxville, Tennessee 37916

NBS-114A (REV. 7-73)

U.S. DEPT. OF COMM. BIBLIOGRAPHIC DATA SHEET	1. PUBLICATION OR REPORT NO. NBSIR 75-659	2. Gov't Accession No.	3. Recipient's Accession No.

4. TITLE AND SUBTITLE
A New Mode of Chipping Fracture in Brittle Solids, and Its Application in a Model for Wear Under Fixed Abrasive Conditions I. Mode of Chipping Fracture II. Wear Model"

5. Publication Date February 1975

6. Performing Organization Code

7. AUTHOR(S)
Brian R. Lawn

8. Performing Organ. Report No.

9. PERFORMING ORGANIZATION NAME AND ADDRESS
NATIONAL BUREAU OF STANDARDS
DEPARTMENT OF COMMERCE
WASHINGTON, D.C. 20234

10. Project/Task/Work Unit No. 3130453

11. Contract/Grant No.

12. Sponsoring Organization Name and Complete Address *(Street, City, State, ZIP)*
Department of the Navy
Office of Naval Research
Arlington, Virginia 22217

13. Type of Report & Period Covered Interim 7/1/74 - 6/30/75

14. Sponsoring Agency Code ONR

15. SUPPLEMENTARY NOTES

16. ABSTRACT *(A 200-word or less factual summary of most significant information. If document includes a significant bibliography or literature survey, mention it here.)*

A description is given of the mode of chipping fracture observed in highly brittle solids. It is pointed out that residual stresses about indentation deformation centers play a vital role. The implications of this mode in a number of mechanical phenomena are discussed.

An explicit model for the wear of brittle surfaces under fixed abrasive conditions is presented in terms of indentation fracture concepts. The predicted wear rate for glass agrees with that observed experimentally to within an order of magnitude. Some implications concerning the parameters which influence the abrasion process, particularly the hardness, are discussed.

17. KEY WORDS *(six to twelve entries; alphabetical order; capitalize only the first letter of the first key word unless a proper name; separated by semicolons)*
Abrasion; brittle solids; brittle surfaces; chipping; fracture; hardness; indentation; residual stress; stress analysis; wear rate

18. AVAILABILITY	19. SECURITY CLASS (THIS REPORT)	21. NO. OF PAGES
☐ Unlimited XXXX For Official Distribution. Do Not Release to NTIS ☐ Order From Sup. of Doc., U.S. Government Printing Office Washington, D.C. 20402, SD Cat. No. C13 ☐ Order From National Technical Information Service (NTIS) Springfield, Virginia 22151	UNCLASSIFIED	29
	20. SECURITY CLASS (THIS PAGE)	**22. Price**
	UNCLASSIFIED	